




## Original Article

# Unveiling MiR-3085-3p as a modulator of cartilage degeneration in facet joint osteoarthritis: A novel therapeutic target

Zhong-ming Lai<sup>1</sup> , Cheng-long Li<sup>1</sup> , Jun-xiong Zhang, Xiang Ao, Cheng-shuo Fei, Xin Xiang, Yan-lin Chen, Ze-sen Chen, Rui-qian Tan, Liang Wang<sup>\*</sup>, Zhong-min Zhang<sup>\*</sup> 

Division of Spine Surgery, Department of Orthopaedics, Nanfang Hospital, Southern Medical University, Guangzhou, China



## ARTICLE INFO

## Keywords:

Endoplasmic reticulum stress  
Facet joint osteoarthritis  
Mechanical stress  
MiR-3085-3p

## ABSTRACT

**Background:** Low back pain (LBP) is generally caused by lumbar degeneration without effective treatment. Lumbar degeneration is influenced by aberrant axial mechanical stress (MS), with facet joint osteoarthritis (FJOA) representing one of its primary pathological manifestations. MicroRNA (miRNA), functioning as an early intermediate in the transcription process, has frequently been demonstrated to serve as a critical mediator linking mechanical stress perception with cellular processes such as growth, development, aging, and apoptosis. We hypothesized that miR-3085-3p regulates chondrocyte apoptosis under mechanical stress, influencing FJOA and serving as a key regulator.

**Methods:** The severity of cartilage degeneration in bipedal standing models (BSM) was established and validated through micro-CT and histopathology. Cyclic tensile strain experiments (CTS) were conducted on the ATDC5 cell line to simulate MS. In situ hybridization was utilized to assess the expression levels of miR-3085-3p in degraded facet articular cartilage. The role of miR-3085-3p and its interaction with the downstream mRNA target Hspb6 were investigated through a combination of bioinformatic analysis, quantitative real-time polymerase chain reaction, western blotting, immunofluorescence, and luciferase assay. In vivo experiments on BSM, the functional impact of miR-3085-3p was further examined through transfection with adeno-associated virus (AAV).

**Results:** It was observed that miR-3085-3p induced endoplasmic reticulum (ER) stress and apoptosis in chondrocytes and cartilage tissues under MS. The detrimental impact of miR-3085-3p was associated with the downregulation of Hspb6 expression, resulting in disruption of endoplasmic reticulum folding function. Additionally, intra-articular transfection of AAV miR-3085-3p mimics in mice facet joints led to spontaneous cartilage loss, while AAV miRNA-3085-3p sponge administration mitigated FJOA in the murine BSM model.

**Conclusion:** Mechanical stress-regulated miR-3085-3p up regulation induced the ER stress and aggravates FJOA development through targeting HSPB6, suggesting miR-3085-3p may be a novel therapeutic target for FJOA. Translational potential of this article: Our study confirmed the elevated expression of miR-3085-3p in lumbar facet joints following mechanical stress loading, suggesting that miR-3085-3p may serve as a biomarker for the clinical management of FJOA. Additionally, we demonstrated that the knockdown of miR-3085-3p in animal facet joints mitigated facet joint degeneration, thereby identifying a potential therapeutic target for FJOA.

## 1. Introduction

Low back pain (LBP) constitutes a significant public health concern on a global scale, with a reported lifetime prevalence among adults reaching up to 84 % [1]. It has emerged as the foremost cause of

disability-adjusted life years (DALYs) for many years [2]. Various etiological factors contribute to LBP, including intervertebral disc degeneration, sacroiliitis, and facet joint syndromes [3]. Notably, facet joint arthropathy, also known as facet joint osteoarthritis (FJOA), is implicated in approximately 30 % of chronic low back pain cases [4,5].

\* Corresponding author. Division of Spine Surgery, Department of Orthopaedics, Nanfang Hospital, Southern Medical University, Guangzhou, China.

\*\* Corresponding author. Division of Spine Surgery, Department of Orthopaedics, The Third Affiliated Hospital of Southern Medical University, Guangzhou, China.

E-mail addresses: [904397475@qq.com](mailto:904397475@qq.com) (Z.-m. Lai), [lclong1203@163.com](mailto:lclong1203@163.com) (C.-l. Li), [3219586627@qq.com](mailto:3219586627@qq.com) (J.-x. Zhang), [aoxiang9212@163.com](mailto:aoxiang9212@163.com) (X. Ao), [fcs2060985@163.com](mailto:fcs2060985@163.com) (C.-s. Fei), [medicalrxiangx1@163.com](mailto:medicalrxiangx1@163.com) (X. Xiang), [y\\_lchen@163.com](mailto:y_lchen@163.com) (Y.-l. Chen), [1059910690@qq.com](mailto:1059910690@qq.com) (Z.-s. Chen), [13580830355@163.com](mailto:13580830355@163.com) (R.-q. Tan), [liang091@aliyun.com](mailto:liang091@aliyun.com) (L. Wang), [nfzzm@163.com](mailto:nfzzm@163.com) (Z.-m. Zhang).

<sup>1</sup> Zhong-ming Lai and Cheng-long Li contributed equally to this work as co-first authors.

<https://doi.org/10.1016/j.jot.2024.11.007>

Received 15 September 2024; Received in revised form 9 November 2024; Accepted 22 November 2024

2214-031X/© 2024 Published by Elsevier B.V. on behalf of Chinese Speaking Orthopaedic Society. This is an open access article under the CC BY-NC-ND license (<http://creativecommons.org/licenses/by-nc-nd/4.0/>).

Contemporary understanding suggests that the pathological alterations observed in FJOA are analogous to those seen in osteoarthritis at large joints at extremities, involving cartilage loss, subchondral bone remodeling, joint space changes, osteophyte formation, ligaments and other imbalances of the entire joint [6,7]. Currently, the management of FJOA predominantly involves non-pharmacological therapies, pharmacological interventions, and intra-articular procedures [8]. Intra-articular interventions include techniques such as intra-articular blockade, radiofrequency ablation denervation, and dorsal root neurectomy [9–11]. The effectiveness of these treatments continues to be a subject of debate. A prospective double-blind randomized controlled trial demonstrated that the conventional treatment of radiofrequency ablation exhibited an efficacy rate of merely 6 % [12]. Moreover, multiple studies have suggested that the effectiveness of intra-articular interventions diminishes over extended follow-up periods, indicating poor long-term efficacy [13–15], as the treatment does not halt the progression of FJOA. Advancements in treatment are contingent upon a deeper understanding of the specific pathogenesis of FJOA and the development of strategies to mitigate cartilage degeneration. Thus, further research on the pathogenesis of this disease and the development of new therapeutics are of great clinical importance.

Mechanical stress, a prevalent *in vivo* stimulus, significantly influences the growth and development of chondrocytes [16,17]. A study has identified mechanical stress as a primary factor contributing to the degeneration of lumbar facet joints. This degeneration occurs because the bilateral facet joints, in conjunction with the intervertebral disc, are responsible for load transfer and the guidance and restriction of spinal movement [18]. To simulate the conditions experienced by facet joints, our research team previously developed a mouse bipedal standing model (BSM) [19]. We observed facet joint degeneration in the BSM in mice subjected to continuous daily weight loading exclusively on the lower limbs. Nevertheless, the precise mechanism by which this alteration in stress induces joint degeneration remains unclear.

MicroRNAs (miRNAs) are a class of endogenous, highly conserved non-coding RNAs approximately 23 nucleotides in length, known to interact with mRNA and suppress its expression within the 3' untranslated region (3'UTR) [20]. miRNAs play a significant role in regulating the homeostasis, growth, and development of chondrocytes, as well as the pathogenesis of osteoarthritis [21]. By establishing mice model of knee OA, Zhang H et al. [22] demonstrated that miR-146a-5p promotes apoptosis in osteoarthritic chondrocytes and inhibits autophagy by targeting NUMB. The regulatory role of miRNAs has been documented not only in large joints but also in small ones like facet joints. Nakamura A et al. [23] demonstrated that antisense oligonucleotides targeting miR-181a-5p effectively mitigated cartilage degeneration in facet joints. Similarly, Zhao J et al. [24] conducted the same animal experiments as the BSM we developed and confirmed that downregulation of miR-325-3p accelerated facet joint chondrocyte aging and exacerbated facet joint degeneration. Recently, Crowe N's research team identified miR-3085-3p as a microRNA predominantly expressed in osteoarthritis chondrocytes [25]. In addition, the team observed that miR-3085-3p plays a role in promoting osteoarthritis by targeting downstream factors [26]. Based on previous studies, miR-3085-3p has been identified as playing a crucial role in OA. Consequently, we hypothesize that miR-3085-3p exerts a similar influence in facet joints. To substantiate this hypothesis, we conducted a preliminary experiment, which revealed that miR-3085-3p was significantly up-regulated in the facet joints following BSM modeling.

Research indicates that chondrocyte apoptosis is notably vulnerable to endoplasmic reticulum (ER) stress due to the critical role of the ER in facilitating cellular functions such as the synthesis and maintenance of the extracellular matrix (ECM) [27]. Various cellular stressors, including mechanical stress, hypoxia, nutrient deprivation, oxidative stress, and aging, can impair the synthesis and secretion of ECM proteins. This impairment may result in the accumulation of aberrant proteins within the ER, thereby inducing ER stress [28]. Prolonged and excessive ER

stress has been shown to activate the apoptotic pathway, indicating that ER stress may contribute to the pathogenesis of cartilage degeneration, such as osteoarthritis [29]. Previous studies have demonstrated that miR-21 modulates ER stress by inhibiting the phosphorylation of p38 MAPK [30]. Additionally, miRs-211-5p and 204-5p have been found to regulate the expression of several ER stress markers downstream of the PERK pathway [31]. Based on previous findings and preliminary experiments, it is plausible to hypothesize that miR-3085-3p may induce degeneration of facet joints in BSM by modulating ER stress and promoting chondrocyte apoptosis.

## 2. Material and method

### 2.1. Establishment of bipedal standing experimental model in mice

All experiments and interventions on animals were approved by the Animal Ethics Committee of Nanfang Hospital, Southern Medical University (IACUC-LAC-20230411-009). Our team has previously established a mouse bipedal standing model (BSM) [19] and observed the development of disc and facet joint degeneration in mice following treatment. For the current study, eighteen 10-week-old male C57BL/6 mice weighted approximately 25g were randomly assigned to either a control group (CON group) or a modeling group (POST 8w group). The mice were placed in specialized molds designed to contain water and provide ventilation. A specific volume of water was added to the mold, ensuring it was positioned 5 mm above the base to induce a fear response of the mice, resulting in upright body position withstanding on two hindlimbs accompanied with raised forelimbs. In contrast, as for the control group, no water was injected into their holding molds. The molding process spanned 8 weeks, with mice exposed to the mold seven days a week for 6 h each day. After standing for 3 h, the technicians moved the mice out of the molding machine, provided them with feed and clean drinking water, and continued to stand after a rest for 2 h. After 8 weeks, the lumbar regions of mice were initially subjected to microCT scanning to generate imaging data. Subsequently, facet joints from six mice (three from the (CON) group and three from the POST 8w group) were used for mRNA sequencing to examine disparities in mRNA expression. Total RNA was isolated from the tissues and sequenced utilizing the Illumina platform (Novaseq 6000 PE150, USA) following quality assurance measures. The remaining mice were euthanized via established cervical dislocation, and the lumbar vertebrae were extracted, preserving the posterior superior iliac spine for identification of the Lumbar 5/Lumbar 6 (L5/L6) segments. All specimens underwent decalcification with an 8 % ethylenediamine tetraacetic acid (EDTA) solution for one month before being embedded in paraffin for histological processing and then analysis.

### 2.2. MicroCT analysis

The isolated facet joints were immobilized in 4 % formaldehyde for a duration of 24 h and subsequently examined through microCT (SCANCO  $\mu$ 80 MicroCT, Switzerland) (voltage, 55 kVp; current, 0.1 mA; and resolution, 12 mm/pixel). The microstructure parameters of the facet joint trabecular bone were assessed by detailing the characteristics of the large joint trabecular bone. Bone volume/total volume (BV/TV) and subchondral bone plate thickness (SBP. Th) were determined using data analysis software (CTAn v1.18, Bruker) and 3-dimensional model visualization software (mCTVol v2.2, Bruker).

### 2.3. *In situ* hybridization (ISH)

MiR-3085-3p expression levels were assessed through *in situ* hybridization (ISH) following the manufacturer's protocol. A specific miR-3085-3p probe was custom-designed and synthesized for this study. Tissue sections were initially dewaxed and hydrated, followed by antigen retrieval through boiling in 0.1M citric acid buffer for 5 min.

Subsequently, protease K was applied at a concentration of 20 units/ml for 10 min at room temperature to facilitate digestion. Permeabilization was achieved by adding 0.2 % Tritonx-100, and endogenous catalase was blocked by incubating the sections with 3 % hydrogen peroxide for 15 min at room temperature. The pre-hybridization solution was subjected to incubation at 37 °C for a duration of 2 h, followed by incubation of the miR-3085-3p-containing hybridization solution overnight at 42 °C. Subsequently, mouse anti-digoxin labeled peroxidase, streptavidin, and tyramine-fluorescein were sequentially introduced. The sections were then sealed using a fluorescent sealer containing DAPI, and the resulting fluorescence images were captured and analyzed using the optical microscope (Zeiss Axio Imager-D2, Germany).

## 2.4. Bioinformatics analysis of mRNA-miRNA interactions

Initially, to identify the genes that significantly contribute to BSM, we conducted transcriptome sequencing on BSM specimens with normal facet joint (NFJ) and degenerative facet joint (DFJ) to screen for differentially expressed genes set (Degs). Next, to identify potential targets of miR-3085-3p, various online databases including miRDB, miR-PathDB, and MicroT-CD were consulted. The predicted miR-3085-3p target genes were intersected with the Degs of the BSM. Venn diagram shows 6 genes that overlap the target genes of Degs and miR-3085-3p.

## 2.5. Luciferase assay

293T cells were plated in 96-well plates and cultured until reaching 70 % confluence. Transfections were performed with 0.16 µg of either m-Hspb6-3'UTR-wt or m-Hspb6 3'UTR-mut, along with 5 pmol of mmu-miR-3085-3p or a negative control, using Lipo3000 (GLPBIO, USA). Cells were harvested and analyzed 48 h post-transfection. The Dual-Luciferase Reporter Assay Kit (Hanbio Biotech, China) was utilized for luciferase activity measurements, with Luciferase Reaction Reagent I detecting firefly luciferase activity and Luciferase Reaction Reagent II measuring Renilla luciferase activity as per the manufacturer's instructions.

## 2.6. Cell culture and transduction

The Murine ATDC5 cell line was procured from KeyGEN BioTECH (Cat#KG445, KeyGEN, China) and maintained in a humidified incubator at 5 % CO<sub>2</sub> and 37 °C using DMEM/F12 (Gibico, US), supplemented with 10 % fetal bovine serum (Procell, China) and 1 % penicillin and streptomycin (Gibico, US). Subsequent to this, the ATDC5 cells were stimulated with insulin-transferring-sodium selenite media supplement (Sigma, USA) to induce their differentiation into chondroblasts [32]. Upon reaching 80–90 percent confluence, the culture medium was replaced.

## 2.7. Cyclic tensile strain (CTS) experiment

To simulate cellular responses to mechanical loading, we conducted *in vitro* experiments involving cell cycle tensile strain on ATDC5 cartilage cell lines seeded onto collagen I biaxial stretch culture plates on a cell tension system (FX5000TXL, Flexcell, USA). The cell tension system utilized in this study was procured from Flexcell, USA, and its mechanical parameters adhere to the original specifications provided by the manufacturer. Upon reaching 80 % confluence, the culture plates were affixed to the piston of a cell tensiometer. The best modeling conditions of ATDC5 cartilage cell line were obtained through preliminary experiments: tensile strength of 20 %, stretching frequency of 0.5 Hz, and duration of 48 h.

## 2.8. Cell transfection and treatments

ATDC5 cells were initially cultured in 6-well plates at a seeding

density of  $1.5 \times 10^5$  cells/well, achieving 80 % confluency within 48 h. Subsequently, the cells were subjected to transfection with miR-3085-3p mimics, scramble, miR-3085-3p inhibitor, and negative control (Sangon Biotech, China) using RNA TransMate at a 4 µl volume as per the manufacturer's protocol. Following a 48-h transfection period, the cells were harvested or continued for other experimentation. As for the target gene Hspb6, an Hspb6 overexpression plasmid (Tsingke Biotech, China) was constructed and utilized for transfection of ATDC5s via Lipo3000 (GLPBIO, USA), following the provided guidelines. The experimental group and procedure were the same as that of miRNA transfection.

## 2.9. RNA extraction and quantitative real-time polymerase chain reaction (qRT-PCR)

Total RNA was isolated from ATDC5s using the TRIzol reagent (Accurate Biology, China). For the miRNA, total RNA (1000 ng) were reverse transcribed into cDNA with miRNA stem loop reverse transcription kit (Sangon Biotech, China) according to manufacturer's instructions. For the mRNA, total RNA (1000 ng) was reverse transcribed into cDNA using HiScript III All-in-one RT SuperMix Perfect for qPCR (Vazyme, China). qRT-PCR was performed using Taq Pro Universal SYBR qPCR Master Mix (Vazyme, China). Cycling conditions are 95 °C for 30 s, followed by 40 cycles of 10s at 95 °C and 30s at 60 °C. Finally, the dissolution curve is programmed to run at 95 °C for 15s, 60 °C for 60s, and 95 °C for 15s. As a standard, all reactions were performed in duplicate and normalized to the internal reference U6 for miRNAs and β-Actin for mRNAs. Relative mRNA/miRNA expression levels were determined using the 2Ct method.

## 2.10. Western blotting

Total proteins were separated from ATDC5s by radio-immunoprecipitation assay buffer (RIPA, Biosharp, China), and protein concentrations were quantified by bicinchoninic acid (BCA) protein assay kit (Solarbio, China). Separating the protein components on sodium dodecyl sulfate polyacrylamide gel electrophoresis (SDS-PAGE) gels and transferring them to polyvinylidene fluoride (PVDF) membranes was performed. After being blocked by 10 mM Tris-buffered saline (TBS) containing 5 % nonfat skimmed milk for 2 h, the membranes were incubated with Anti-Mmp13 antibody (1:1000, Affinity, #AF5355), Anti-Adams5 antibody (1:1000, Affinity, #DF13268), Anti-Hspb6 antibody (1:1000, Affinity, #AF6003), Anti-Atf4 antibody (1:1000, Affinity, #DF6008), Anti-Grp78 antibody (1:1000, Abcam, #ab108615), Anti-Cleaved caspase3 (1:1000, Cell Signaling, #9664S), Anti-Bcl2 (1:1000, Affinity, #AF6139), Anti-Gapdh antibody (1:5000, Affinity, #AF7021), Anti-β-Tubulin (1:1000, Affinity, #DF7967), Anti-β-Actin antibody (1:10000, Affinity, #T0022) at 4 °C for 14–16 h, washed by TBS with Tween-20 (TBST), followed by secondary antibody (Goat Anti-Rabbit IgG, 1:5000, Affinity, #S0001; Goat Anti-Mouse IgG, 1:5000, #S0002) incubation for 1 h at room temperature. Membranes were excited by a hypersensitive ECL chemiluminescence kit and placed into BCL chemiluminescence instrument to record the trend of protein blot expression.

## 2.11. Immunofluorescence staining

The ATDC5 cell line was suspended and seeded onto a 6-well plate, following successful transfection and experimental treatments. The cells were fixed with 4 % paraformaldehyde for 15 min, permeabilized with 0.2 % Tritonx-100 for 10 min, and blocked with 5 % BSA at room temperature for 30 min. Subsequently, the primary antibody was incubated overnight at 4 °C, followed by incubation with the secondary antibody in the dark for 1 h. The antibodies were anti-Hspb6 (1:200, Affinity, #AF6003) and Goat Anti-Rabbit IgG (H + L) FITC-conjugated (1:200, Affinity, #S0008), respectively. The cell slides were extracted using microscopic forceps and sealed with 4',6-diamidino-2-phenylindole (DAPI) fluorescent sealer. Fluorescence images were obtained

using optical microscope (Zeiss Axio Imager-D2, Germany).

### 2.12. Apoptosis detection

Flow cytometry was used to measure cell apoptosis. The ATDC5 transfection assay was conducted in a 6-well plate using EDTA-free pancreatic enzyme digestion to harvest cell precipitates. Following the protocol of the Annexin V-Abfluor 488/PI double-stained apoptosis detection kit, the Annexin V working solution was incubated for 15 min in the absence of light, and apoptosis was assessed using flow cytometry (BECKMAN, flow cytometer Cytoflex, USA). It is noteworthy that the Hspb6 overexpression plasmid emits green fluorescence, necessitating the use of the Annexin V-IF647/PI apoptosis detection kit for detecting apoptosis in experimental cells transfected with Hspb6 overexpression [33].

### 2.13. Animal transfection experiment

MiR-3085-3p overexpression and knockdown adeno-associated virus (AAV) were designed and synthesized to complete animal transfection experiments. A total of 24 10-week-old male C57B/L6 mice were randomly divided into 4 groups, including: negative control group (AAV NC), overexpression group (AAV mimics), negative control with BSM (AAV NC + POST 8w), and knockdown group with BSM (AAV sponge + POST 8w). The facet joints of mice were injected with AAV *in situ*. In the initial phase of the experiment, mice were anesthetized using isoflurane and a precise incision was performed at the juncture of the posterior superior iliac spine and the central spine axis following disinfection, resulting in the exposure of the L5/L6 facet joints. Adeno-associated viruses (AAV) were administered using a Hamilton microsyringe, ensuring a copy number of  $10^{12}$  genome copies (GC) in each joint. Subsequently, the subcutaneous tissue and skin were sutured. After a period of 2 weeks, the BSM was constructed in AAV NC + POST 8w group and AAV sponge + POST 8w group. After 8 weeks, all mice were euthanized and specimens from the L5/L6 region were collected for further analysis.

### 2.14. Histological analysis

After fixation, decalcification, dehydration, and embedding, the collected lumbar spine specimens were prepared into 4  $\mu$ m tissue sections, which were dewaxed and hydrated before staining. For hematoxylin and eosin (H&E) staining, the pre-prepared slices were soaked with hematoxylin (Biosharp, China) for 2 min, differentiated with 1 % hydrochloric acid solution for 2 s, and eosin (Biosharp, China) impregnated for 5 min; For Safranin O-Fast Green staining, the nucleus was first stained with hematoxylin, followed by 0.05 % fast green (Sigma, USA) for 8 min, 0.1 % Safranin O (Sigma, USA) for 5 min; To perform immunohistochemistry, specimens were repaired by antigen, peroxidase was blocked, and specimens were sealed, and then incubated overnight at 4 °C with primary antibodies. The primary antibodies involved in this study include Anti-Mmp13 antibody (1:200, Affinity, #AF5355), Anti-Adams5 antibody (1:200, Affinity, #DF13268) Anti-Hspb6 antibody (1:200, Affinity, #AF6003), Anti-Atf4 antibody (1:200, Affinity, #DF6008), Anti-Grp78 antibody (1:200, Abcam, #ab108615). The secondary antibody (Goat Anti-Rabbit IgG, 1:400, Affinity, #S0001) was incubated at room temperature for 2 h. DAB staining was performed with DAB chromogenic kit (Solarbio, China), and hematoxylin staining was performed after observing the gene expression trend. For all histological staining, sections were sealed with clear, neutral paraffin after staining.

### 2.15. Statistical analysis

GraphPad Prism 8.0 software was used for data analysis and quantitative data were presented as Mean  $\pm$  SD. The Student's t-test was

employed to assess differences between two independent groups, while one-way ANOVA followed by Tukey's post hoc tests was used to differences between multiple groups. Significance was set at a level of  $p < 0.05$ . Animal experiments were repeated with a minimum of 6 samples, while cell experiments were repeated with a minimum of 3 samples.

## 3. Result

### 3.1. Elevated miR-3085-3p in degenerative lumbar facet joints

To investigate the correlation between miR-3085-3p expression and degenerated lumbar facet joints, a mouse BSM was established and divided into control (CON) and modeling groups (POST 8w). Imaging analysis revealed a significant increase in subchondral bone mass in the POST 8w group, as evidenced by 3-D reconstruction of subchondral bone in facet joints (Fig. 1c). Furthermore, BV/TV (Fig. 1a) and SBP.Th (Fig. 1b) in the POST 8w group exhibited a notable increase following 8 weeks of modeling, suggesting an augmentation in bone mass and increase in subchondral bone thickness of lumbar facet joints. Histological analysis revealed changes in cartilage morphology and discontinuities in the POST 8w group, as demonstrated by H&E staining (Fig. 1d). Safranin O/Fast green staining in the same group indicated cartilage matrix loss and an elevated Osteoarthritis Research Society International (OARSI) score, both indicative of cartilage degeneration (Fig. 1g, i). ISH showed a significant increase in fluorescence intensity of miR-3085-3p probe in the degraded cartilage of the POST 8w group (Fig. 1h–i). Immunohistochemistry also showed an increased expression of Mmp13 and Adams5 genes in the cartilage tissue of the POST 8w group (Fig. 1d), and the statistics of positive cells (Fig. 1e and f).

### 3.2. Increased expression of miR-3085-3p in chondrocytes under abnormal mechanical stress (MS)

This study utilized the cyclic tensile strain (CTS) assay on the ATDC5 cartilage cell line to investigate the correlation between miR-3085-3p expression and mechanical loading. Findings from qRT-PCR and Western Blot analyses indicated a degenerative effect on ATDC5 cells under CTS conditions, as evidenced by elevated levels of Mmp13 and Adams5 (Fig. 2b–d). The statistical diagram of protein detection is shown in Supplementary Figs. 4a–b. Furthermore, qRT-PCR results demonstrated an upregulation of miR-3085-3p expression in ATDC5 cells subjected to CTS, supporting the notion that miR-3085-3p was responsive to mechanical stress, as depicted in Fig. 2a. Fig. 2e displays the outcomes of flow cytometric apoptosis assessment following the application of mechanical loading on ATDC5 cells. The imposition of mechanical stress notably elevated the Q2+Q3 ratio in the CTS group as opposed to the control group, suggesting the occurrence of apoptosis in ATDC5 cells. The distribution of early and late apoptotic cells in the CTS group is illustrated in Fig. 2f.

### 3.3. MiR-3085-3p induces endoplasmic reticulum stress (ER stress) and leads to chondrocyte apoptosis

In the scope of this research, we developed and synthesized sequences for the expression and suppression of miR-3085-3p for transfection experiments on ATDC5 cells to further explore its involvement in ER stress and apoptosis. Initially, the results depicted in Fig. 3a–b demonstrated a substantial 6000-fold increase in miR-3085-3p expression following mimics transfection, with a subsequent decrease observed after inhibitor transfection, thus confirming the efficacy of the transfection process. Subsequently, ATDC5 cells were subjected to treatment with or without CTS in the presence of miR-3085-3p mimics or inhibitors. In the case of excessive mechanical load, the introduction of miR-3085-3p mimics led to a notable upregulation in the expression levels of ER stress target genes Atf4, Grp78, and apoptosis-related genes Cleaved caspase3, while concurrently downregulating the expression of

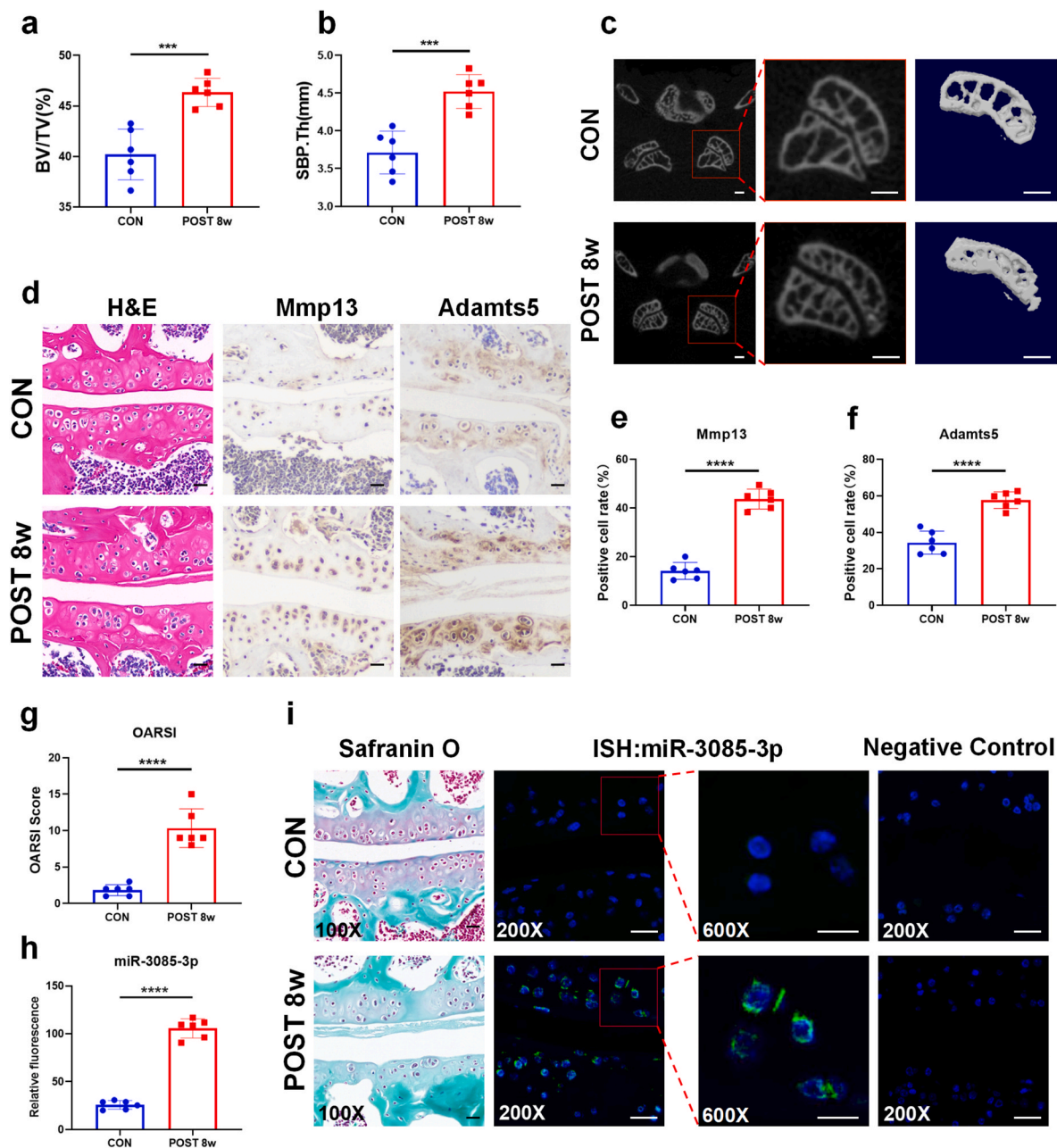


**Fig. 1.** Elevated MiR-3085-3p was found in degenerative lumbar facet joints in mice. (a) Statistical analysis of BV/TV between the control (CON) group and the bipedal standing model (BSM) group. (b) Statistical analysis of SBP.Th between the CON group and the BSM group. (c) CT view and 3D reconstruction view of the CON group and the BSM group. Scale bars, 500  $\mu$ m. (d) H&E staining (left panel) and immunohistochemistry image (right panel) of Mmp13 and Adamts5 between the CON group and the BSM group. Scale bars, 50  $\mu$ m. (e, f) Statistical graph of expression of Mmp13 and Adamts5 detected by immunohistochemistry. (g) OARSI scoring statistical analysis between the CON group and the BSM group. (h) In situ hybridization (ISH) fluorescence intensity statistics between the CON group and the BSM modeling group. (i) Safranin O/fast green staining (left panel) and ISH (right panel) of the cartilage between the CON group and the BSM group. Scale bars, 50  $\mu$ m. \*\*\* $P < 0.001$ , \*\*\*\* $P < 0.0001$ . All data are shown as means  $\pm$  SDs of six independent experiments in (a) (b) (e) (f) (g) (h), student's t-test was used for comparison between two groups. (For interpretation of the references to colour in this figure legend, the reader is referred to the Web version of this article.)

the apoptosis-protecting gene Bcl2 (Fig. 3c–f). In contrast, the inhibition of miR-3085-3p was able to reverse these trends (Fig. 3g–j). MiR-3085-3p promotes ER stress and cell apoptosis at the protein level under abnormal mechanical stress, supporting mRNA expression levels' outcome (Fig. 3k–n). To further investigate the impact of miR-3085-3p on chondrocyte apoptosis induced by mechanical stress, flow cytometry was utilized to assess apoptosis in cells transfected with miR-3085-3p mimics and inhibitor. The findings indicated that upregulation of miR-3085-3p exacerbated apoptosis in ATDC5 cells, whereas down-regulation of miR-3085-3p partially reversed apoptosis in ATDC5 cells

under abnormal mechanical load, as depicted in Fig. 3o–q. In conclusion, these results suggest that miR-3085-3p induces ER stress, which leads to apoptosis. Following the confirmation that overexpression of miR-3085-3p induces apoptosis in chondrocytes, we investigated whether the simple inhibition of miR-3085-3p would impact the normal functioning of these cells. The results indicated that, on the third- and fifth-days post-transfection of ATDC5 cells with the miR-3085-3p inhibitor, there were no significant changes in the expression levels of chondrocyte marker genes Col2a and Sox9. Additionally, there was no upregulation of extracondral matrix degradation marker genes Mmp13 and Adamts5, as

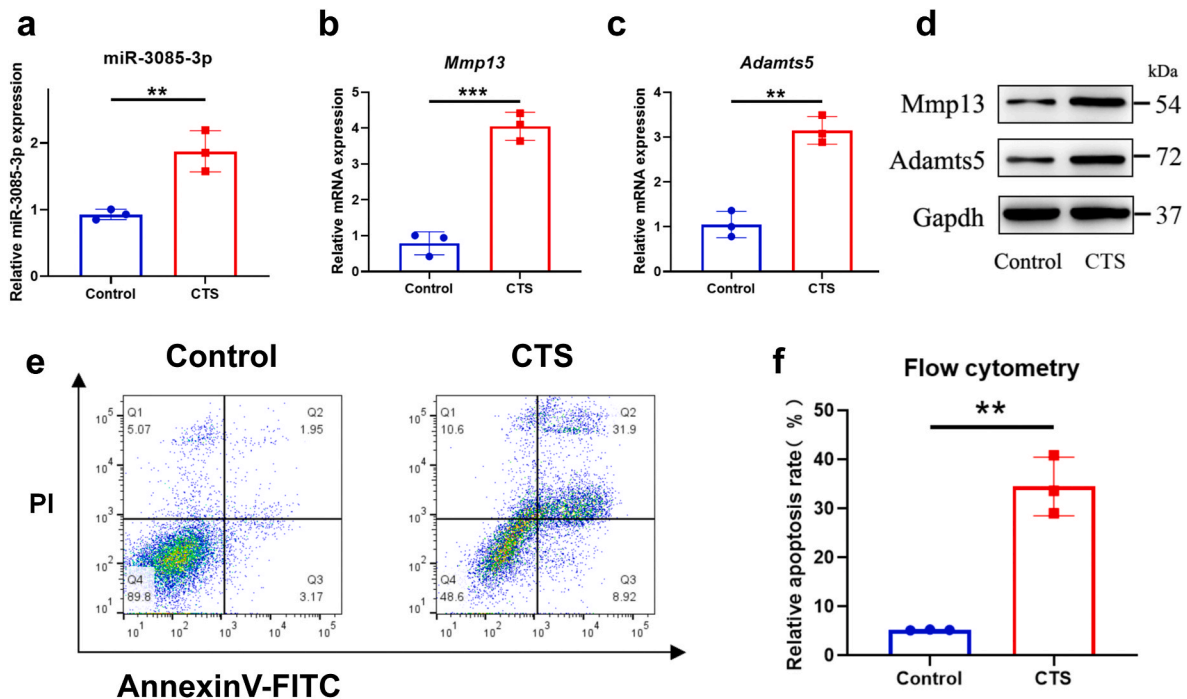


**Fig. 2.** The expression of miR-3085-3p was increased in chondrocytes stimulated by mechanical stress. Cyclic tensile strain (CTS) test was carried out on ATDC5, and the load condition of CTS group molding was 20 % strength, 0.5Hz, 48h. (a–c) qRT-PCR analysis of miR-3085-3p(a), Mmp13(b), Adamts5(c) expression between control group and CTS group. (d) Western blotting analysis of Mmp13 and Adamts5 protein levels between control group and CTS group. (e) Flow cytometry was used to detect the amount of apoptosis in control group and CTS group. (f) The statistical graph of the number of apoptosis detected by flow cytometry. \*\* $P < 0.01$ , \*\*\* $P < 0.001$ . All data are shown as means  $\pm$  SD of three independent experiments in (a) (b) (c) (f), student's t-test was used for comparison between two groups.

illustrated in [Supplementary Fig. 1a–d](#).

### 3.4. miR-3085-3p directly targets Hspb6

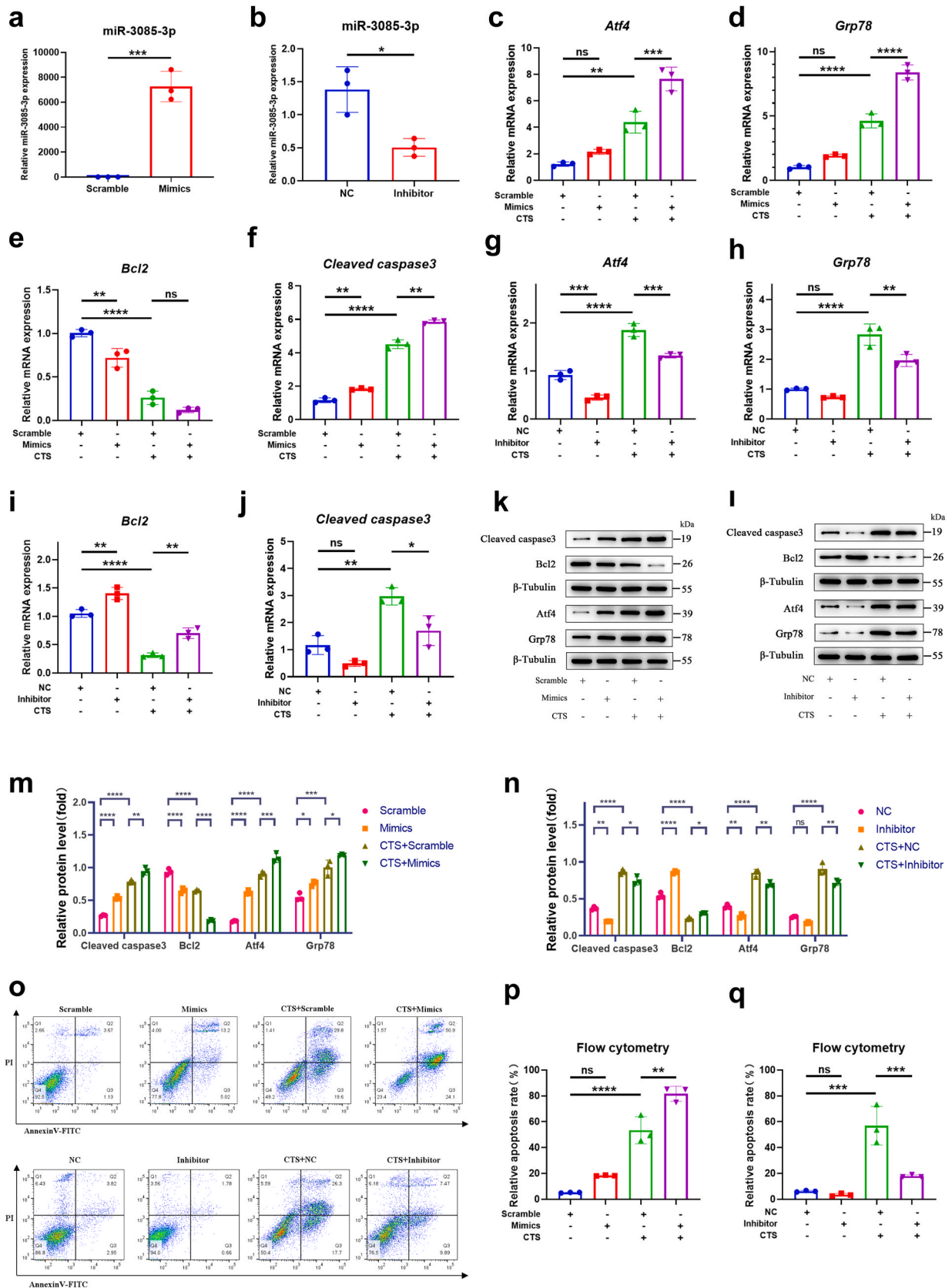
A comprehensive analysis utilizing BSM transcriptome sequencing identified a total of 413 differentially expressed genes (fold-change = 1.5,  $p < 0.05$ , FDR < 1), forming the differentially expressed gene set (Degs). In order to investigate potential miR-3085-3p target genes associated with Degs identified through transcriptome sequencing of BSM mRNA, bioinformatics analysis was conducted using public databases such as miRDB, MiRPathDB, and MicroT-CDs. A total of 269 miR-3085-3p target genes were identified from the public dataset ([Fig. 4a](#)), and 6 key genes were further identified through intersection with Degs ([Fig. 4b](#)). The expression levels of these 6 key genes in the Degs matrix are depicted in a heat map in [Fig. 4c](#), with Hspb6 exhibiting the highest expression level. Therefore, it is suggested that Hspb6 may play a crucial role in the regulation of miR-3085-3p and the development of facet joint degeneration. The results of western blotting and qRT-PCR analyses indicated a negative correlation between Hspb6 mRNA and protein (Hspb6) levels and miR-3085-3p expression in ATDC5 cells, both with and without CTS modeling ([Fig. 4f–i](#)). The statistical diagram of protein detection is shown in [Supplementary Figs. 4c–d](#). Immunofluorescence assays consistently demonstrated that miR-3085-3p significantly suppressed the expression of Hspb6 ([Fig. 4j–l](#)). In accordance with target prediction algorithms, miR-3085-3p was identified as a target for mouse Hspb6 3'UTRs, which contained possible seed sequences ([Fig. 4d](#)). In order to confirm the direct binding of miR-3085-3p with the 3'UTR of Hspb6 mRNA, a luciferase activity assay was conducted. The results showed that miR-3085-3p mimics significantly inhibited the luciferase activity of the reporter gene in cells transfected with the wild type (WT) 3'UTR of Hspb6, but not in cells transfected with the mutated (Mut) 3'UTR of Hspb6 ([Fig. 4e](#)). These findings suggest that miR-3085-3p directly targets Hspb6 in chondrocytes.

### 3.5. miR-3085-3p induces ER stress leading to apoptosis by targeting Hspb6

To further confirm the role of miR-3085-3p in exacerbating FJOA through the targeting of Hspb6, we conducted a response experiment involving the overexpression of Hspb6 in ATDC5 cells via transfection with plasmids containing Hspb6 overexpression (Hspb6 OE). The transfection efficiency of Hspb6 OE was verified at transcriptional and protein levels ([Fig. 5a](#), [Supplementary Fig. 4e](#)). In the situation of abnormal mechanical stress, co-transfection of miR-3085-3p mimics and Hspb6 OE into ATDC5 cells resulted in the reversal of the effects of miR-3085-3p overexpression on the down-regulation of Bcl2 expression and the upregulation of Atf4, Grp78, and Cleaved caspase3 expression, as determined by qRT-PCR ([Fig. 5b–e](#)). The findings indicate a consistent pattern in protein levels, wherein the overexpression of Hspb6 partially counteracted the upregulation of Atf4, Grp78, Cleaved caspase3, and the downregulation of Bcl2 induced by miR-3085-3p ([Fig. 5f–g](#)). Additionally, flow cytometry analysis revealed a reduction in apoptotic cells following Hspb6 overexpression in response to miR-3085-3p under overload stress ([Fig. 5h–i](#)). Our experimental data further supports the notion that miR-3085-3p exacerbates ER stress-induced apoptosis by targeting Hspb6.

### 3.6. Down-regulation of miR-3085-3p in mouse facet joints alleviates the exacerbation of FJOA

Mice in the control group were transfected with AAV-miR-3085-3p mimics (or NC), while BSM mice (POST 8w) were transfected with AAV-miR-3085-3p sponge (or NC) to investigate the role of miR-3085-3p during the progression of FJOA. To assess AAV transfection effectiveness, qRT-PCR measured miR-3085-3p expression post-transfection with AAV mimics or sponge. After one week, changes in miR-3085-3p levels were minimal, but significant up-regulation ([Supplementary Fig. 2a](#)) or down-regulation ([Supplementary Fig. 2b](#)) was observed after



(caption on next page)

**Fig. 3.** miR-3085-3p induces endoplasmic reticulum stress (ER stress) and leads to chondrocyte apoptosis. (a,b) ATDC5s were transfected with miR-3085-3p mimics (a) or scramble and miR-3085-3p inhibitor(b) or negative control (NC). After 48 h of transfection, miR-3085-3p levels in ATDC5s were evaluated by qRT-PCR. Cyclic tensile strain (CTS) test was performed after transfection, and the load condition of CTS group molding was 20 % strength, 0.5Hz, 48h. (c–f) qRT-PCR analysis of Atf4 (c), Grp78 (d), Bcl2 (e) and Cleaved caspase3 (f) in ATDC5s transfected with miR-3085-3p mimics or scramble with or without CTS. (g–j) qRT-PCR analysis of Atf4 (g), Grp78 (h), Bcl2 (i) and Cleaved caspase3 (j) in ATDC5s transfected with miR-3085-3p inhibitor or NC with or without CTS. (k, l) Western blotting analysis of Atf4, Grp78, Cleaved caspase3 and Bcl2 protein levels in ATDC5s after miR-3085-3p overexpression (k) and inhibition (l). (m, n) Quantification data of Western blotting analysis of Atf4, Grp78, Cleaved caspase3 and Bcl2 protein levels after miR-3085-3p inhibition (n) and overexpression (m). (O) Flow cytometry was used to detect the amount of apoptosis after miR-3085-3p inhibition and overexpression with or without CTS. (p, q) The statistical graph of the number of apoptosis detected by flow cytometry. ns: no significant difference, \*P < 0.05, \*\*P < 0.01, \*\*\*P < 0.001, \*\*\*\*P < 0.0001. All data are shown as means ± SD of three independent experiments in (a) (b) (c) (d) (e) (f) (g) (h) (i) (j) (m) (n) (p) (q), student's t-test and one-way analysis of variance (ANOVA) were used for comparison between two groups and multiple groups, respectively.

two weeks, confirming effective AAV transfection. Imaging analysis indicated an increase in bone mass and thickness of the subchondral bone in facet joints following transfection with AAV-miR-3085-3p mimics. Conversely, the application of AAV-miR-3085-3p sponge to attenuate miR-3085-3p expression effectively reversed the observed increase in bone mass and thickness in the subchondral bone of BSM mice, micro CT images are presented in [Supplementary Fig. 3a-d](#), 3D reconstruction view and statistical analyses chart are depicted in [Fig. 6a, g, h](#). Histological analysis using H&E staining, Safranin O, and Fast Green staining revealed that AAV-miR-3085-3p mimics induced cartilage destruction in a spontaneous manner, whereas inhibition of miR-3085-3p attenuated the progression of FJOA in BSM mice following injection of AAV-miR-3085-3p sponge ([Fig. 6b, c, i](#)). Subsequently, we confirmed *in vivo* that Hspb6 is a downstream target of miR-3085-3p. Immunohistochemical analysis revealed a decrease in Hspb6 expression with overexpression of miR-3085-3p, and an increase in Hspb6 expression with knockdown of miR-3085-3p ([Fig. 6d, j](#)). To evaluate the impact of miR-3085-3p on cartilage ER stress, the expression of Atf4 and Grp78 was examined. It was observed that the administration of AAV-miR-3085-3p mimics exacerbated ER stress by upregulating Atf4 and Grp78 in FJOA, whereas AAV-miR-3085-3p sponge attenuated ER stress by decreasing Atf4 and Grp78 in FJOA, as evidenced by immunohistochemical analysis ([Fig. 6e, f, k, l](#)). The results of these studies suggest miR-3085-3p can aggravate joint degeneration by increasing ER stress to promote articular cartilage apoptosis *in vivo*.

#### 4. Discussion

The scientific hypothesis of this study is systematically validated through a series of experimental steps. Initially, we identified miR-3085-3p as a significant factor in the initiation and progression of FJOA. Subsequently, our predictions and validations identified Hspb6 as a definitive target gene of miR-3085-3p. Furthermore, our investigations revealed that miR-3085-3p modulates key genes associated with ER stress and apoptosis. Recovery experiments demonstrated that Hspb6 can counteract the regulatory effects of miR-3085-3p. Finally, we also confirmed that the suppression of miR-3085-3p mitigated the progression of FJOA in murine facet joints. In summary, the upregulation of miR-3085-3p induced by mechanical stress precipitates ER stress and apoptosis through its interaction with Hspb6 ([Fig. 6m](#)). Consequently, targeting miR-3085-3p may represent a promising therapeutic strategy for the prevention and treatment of FJOA.

As a highly conserved non-coding RNA, miRNA interacts with homologous messenger RNA (mRNA) to perform its primary function [34]. As a highly conserved non-coding RNA, miRNA interacts with homologous messenger RNA (mRNA) to perform its primary function. Excessive mechanical load has become an important risk factor for joint degeneration [35]. A number of studies have demonstrated that microRNAs are implicated by mechanical stress. Research has shown that miR-221 and miR-222 may act as regulators of mechanotransduction pathways in bovine cartilage, as evidenced by their increased expression in the anterior weight-bearing area compared to the posterior non-weight-bearing region [36]. Furthermore, miR-365 has been implicated in cartilage catabolism through its modulation of mechanical

stress and pro-inflammatory responses [37]. Additionally, miR-146a has been found to upregulate vascular Endothelial Growth Factor (VEGF) by downregulating Smad4 under mechanical stress, ultimately resulting in apoptosis of human chondrocytes [38]. In particular, the study by Zhao J's team demonstrated that miR-325-3p can be down-regulated by mechanical loading in the facet joints [24]. Previous studies have shown a strong association between miR-3085-3p and osteoarthritis [26]. Nevertheless, the impact of mechanical loading on miR-3085-3p and the precise mechanisms underlying cartilage degeneration remain uncertain. In this study, we found that miR-3085-3p has the effect of aggravating cartilage degeneration. Under excessive mechanical loading, the overexpression of miR-3085-3p increased the expression of ER stress related target genes, such as Atf4 and Grp78, and promoted apoptosis through upregulation of Cleaved caspase3 and downregulation of Bcl2. Therefore, we believe that this is the first report that highlights the biological significance of miR-3085-3p in FJOA exacerbation.

Small heat shock proteins (sHsps) are a widespread chaperone family characterized by core domains of crystalline proteins containing 80–100 amino acid residues. In Human tissues, HSPB6 (HSP20) and HSPB1 (HSP27) are major members of small heat-shock proteins family [39]. Under stressful conditions, these sHsps are overexpressed to prevent protein aggregation and apoptosis [40]. The endoplasmic reticulum (ER) is a crucial organelle involved in the synthesis, folding, and maintenance of proteins and lipids, as well as cellular homeostasis. Dysfunction of the ER can result in ER stress, which has been implicated in various pathological conditions. Studies have shown that several sHsps are localized to the ER and play a protective role in mitigating ER stress [41]. HSPB6 phosphorylation on serine16 protects against oxygen-glucose deprivation and reperfusion-induced ER structural changes in Human neuroblastoma (SH-SY5Y) cells via ER stress [42]. In addition, studies have shown that KAIIV, a peptide homologous to the a crystal protein sequence in HSPB6, can inhibit the apoptosis of HeLa cells by blocking the release of mitochondrial cytochrome c and the activation of caspase-3 [43]. According to our study, miR-3085-3p has the potential to target multiple downstream genes. However, our results suggest that miR-3085-3p is related to mechanical load, and could directly target Hspb6, which could inhibit ER stress and apoptosis. Furthermore, miR-308-3p regulated Hspb6 downregulation in the cartilage degeneration area. Overexpression of Hspb6 significantly reversed the ER stress and apoptosis caused by miR-3085-3p mimics, confirming that Hspb6 was the direct target of miR-3085-3p to suppress cartilage degeneration. Therefore, identifying miR-3085-3p's role in FJOA prevention and treatment will shed light on the disease.

The degeneration of facet joints, particularly in the lumbar spine, has garnered increased attention due to its potential occurrence independent of disc degeneration [44]. The facet joint, situated in the posterior column of the lumbar spine, exhibits a greater range of motion that can lead to significant degeneration. Additionally, rodents experience differing axial forces on their spines compared to humans [45]. This study utilized a BSM in which the orientation of the mouse's facet joint was altered to align parallel to the horizontal plane, as opposed to perpendicular. This modification was made to better mimic the stress conditions experienced by humans. BSM are considered to be more representative of real-life scenarios compared to other invasive models



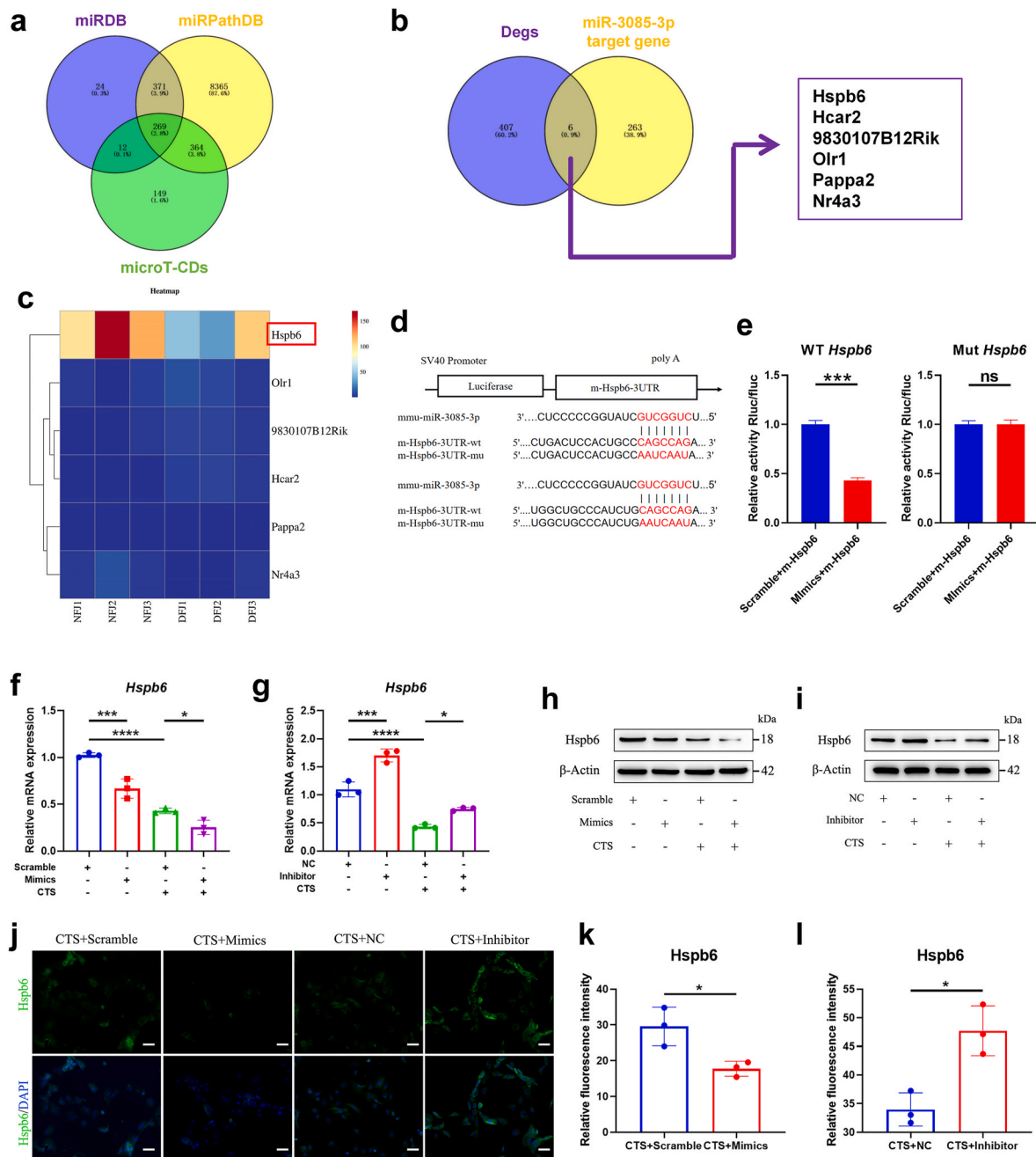


**Fig. 4.** Identification of Hspb6 as a direct target of miR-3085-3p in ATDC5s. (a) Venn diagram display the overlapping of the mice target genes of miR-3085-3p, as predicted by miRDB, miRPathDB and microT-CDs starbase. (b) Venn diagrams display the overlapping miR-3085-3p target genes and transcriptome sequencing differential gene set (Degs) caught from the mRNA sequencing of bipedal standing model. (c) Heat map of 6 genes after intersection of MiR-3085-3p and Degs. (d) A sequence alignment of a putative miR-3085-3p binding site within the 3'UTR of Hspb6 mRNA shows high sequence conservation and complementarity. (e) HEK-293T cells were co-transfected with miR-3085-3p mimics or scramble and luciferase reporter constructs of the wild-type Hspb6-3'UTR (3'UTR-wt) or the mutated Hspb6-3'UTR (3'UTR mut). After transfection, luciferase activity was measured. Luciferase reporter assay revealed that miR-3085-3p exclusively decreased luciferase activity of the wild-type reporter plasmids. ATDC5s were transfected with miR-3085-3p mimics(a) or scramble and MiR-3085-3p inhibitor (b) or negative control (NC). A cyclic tensile strain (CTS) test was performed after transfection, and the load condition of CTS group molding was 20 % strength, 0.5Hz, 48h. (f,g) qRT-PCR analysis of Hspb6 transfected with miR-3085-3p mimics(f) or inhibitor(g) with or without CTS. (h,i) Western blotting analysis of Hspb6 protein levels in ATDC5s after miR-3085-3p overexpression (h) and inhibition(i) with or without CTS. (j) Representative images of Hspb6 assayed by immunofluorescence confocal microscopy in ATDC5s with miR-3085-3p knockdown or overexpression with CTS. DAPI, 4',6-diamidino-2-phenylindole. Scale bar, 50  $\mu$ m. (k,i) Quantification of positive cells after miR-3085-3p overexpression(k) or inhibition (i) with CTS. ns: no significant difference, \*P < 0.05, \*\*\*P < 0.001, \*\*\*\*P < 0.0001. All data are shown as means  $\pm$  SD of three independent experiments in (e) (f) (g) (k) (l), student's t-test and one-way analysis of variance (ANOVA) were used for comparison between two groups and multiple groups, respectively.

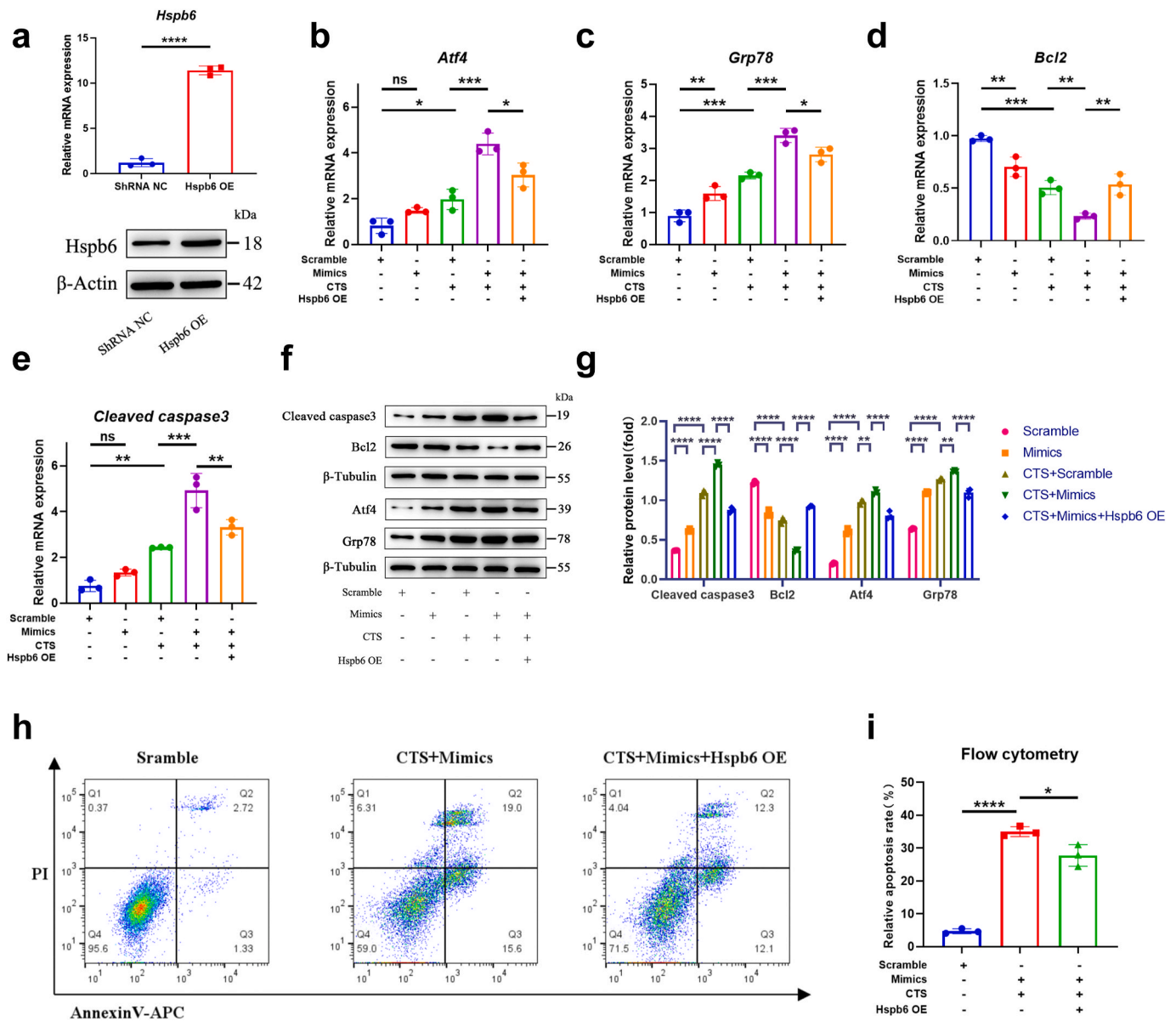


**Fig. 5.** MiR-3085-3p induces ER stress leading to apoptosis by targeting Hspb6. (a) ATDC5s were transfected with Hspb6 overexpression plasmid. After 48h of transfection, qRT-PCR and Western blotting analysis of Hspb6 were performed. (b–e) ATDC5s were transfected with miR-3085-3p mimics or scramble combine with Hspb6 overexpression plasmid. After 48h of transfection, Cyclic tensile strain (CTS) test was performed, and the load condition of CTS group molding was 20 % strength, 0.5Hz, 48h. qRT-PCR analysis of Atf4 (b), Grp78 (c), Cleaved Caspase3 (d) and Bcl2 (e) in ATDC5s after transfection with a combination of miR-3085-3p mimics and Hspb6 overexpression with or without CTS. (f) Western blotting analysis of Atf4, Grp78, Cleaved caspase3, Bcl2 protein levels in ATDC5s with a combination of miR-3085-3p mimics and Hspb6 overexpression with or without CTS. (g) Quantification data of western blotting analysis of Atf4, Grp78, Cleaved caspase3 and Bcl2 protein levels after transfection with a combination of miR-3085-3p mimics and Hspb6 overexpression with or without CTS. (h) Flow cytometry was used to detect the number of apoptosis after transfection with a combination of miR-3085-3p mimics and Hspb6 overexpression with or without CTS. (i) The statistical graph of the number of apoptosis detected by flow cytometry. ns: no significant difference, \*P < 0.05, \*\*P < 0.01, \*\*\*P < 0.001, \*\*\*\*P < 0.0001. All data are shown as means ± SD of three independent experiments in (a) (b) (c) (d) (e) (g) (i), student’s t-test and one-way analysis of variance (ANOVA) were used for comparison between two groups and multiple groups, respectively.

of facet degeneration [23,46]. The indicators pertaining to cartilage degeneration of the BSM exhibited positive results following modeling, thereby enhancing the efficacy of the modeling process. Additionally, intraarticular injections were utilized to introduce AAV carrying either an overexpression or knockdown of miR-3085-3p. Our result revealed that the overexpression of miR-3085-3p exacerbated FJOA in growing mice, whereas a reduction in miR-3085-3p levels improved the degenerated cartilage in the BSM without affecting the normal function of the cells. Consequently, blocking miR-3085-3p appears to be a promising treatment for FJOA according to our study with good clinical translational value.

A few limitations are evident in our study. Firstly, based on miRbase data, miR-3085-3p exhibits homology with both humans and mice. However, our research solely focused on investigating the impact of miR-3085-3p on chondrocytes in mice, without extending the analysis to human specimens and cells. Secondly, while exploring the regulatory axis of miR-3085-3p/Hspb6/FJOA, we did not consider the potential influence of other cellular factors on miR-3085-3p, such as H3K4me3 demethylase and SnoRNAs. Furthermore, our investigation confirmed that miR-3085-3p facilitates ER stress and apoptosis through its interaction with Hspb6. However, the precise mechanisms by which Hspb6 modulates ER stress, apoptosis, and cartilage degeneration remain to be

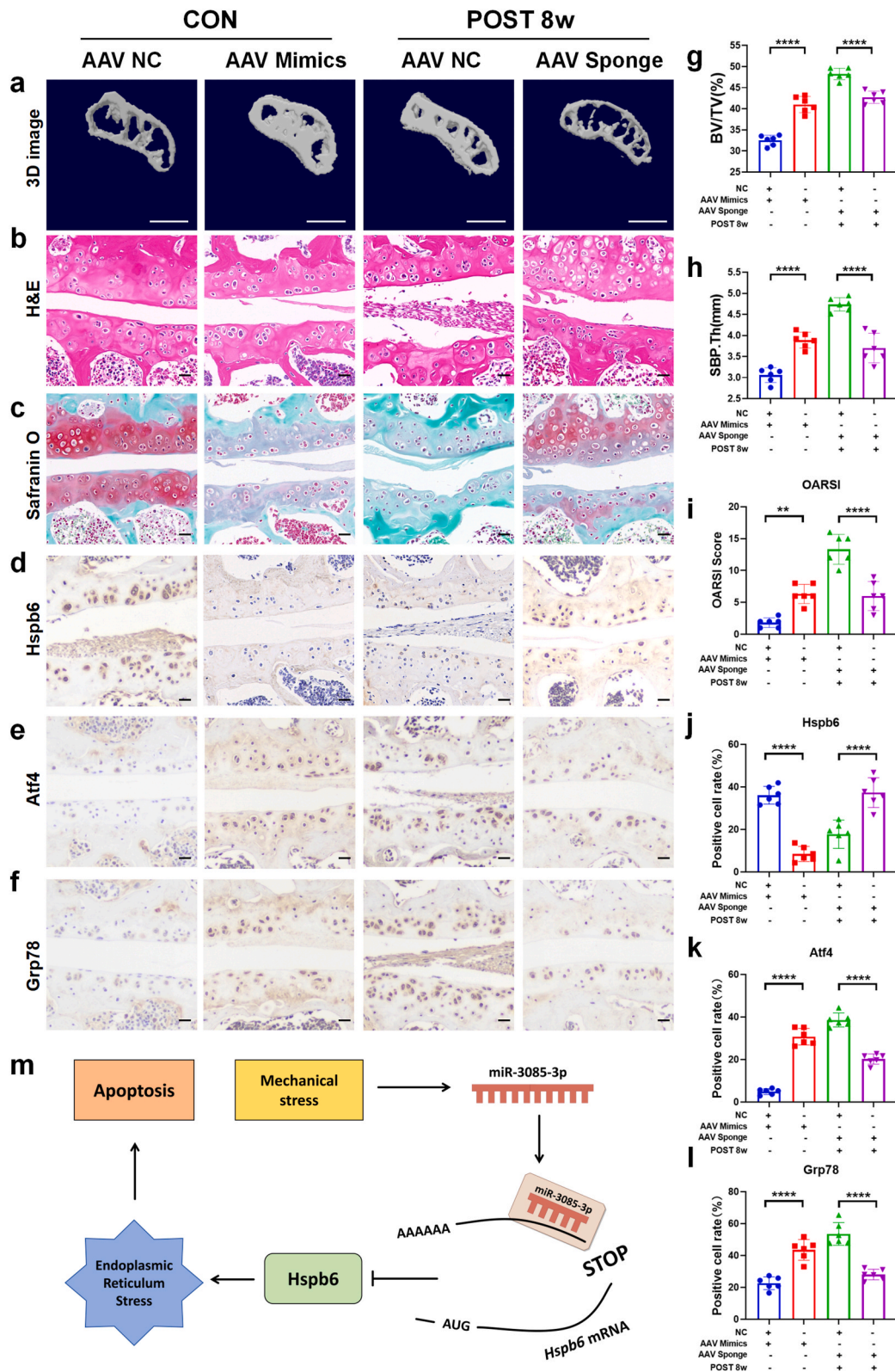


**Fig. 6.** MiR-3085-3p aggravates facet joint osteoarthritis *in vivo*. Mice in control group were injected with adeno-associated virus (AAV) miR-3085-3p mimics or AAV NC, while experiencing bipedal standing model (BSM) mice were injected with AAV-miR-3085-3p sponge or AAV NC. (a) 3D reconstruction view were created using Micro CT, Scale bars, 500  $\mu$ m. (b,c) The articular cartilage was stained with Hematoxylin/Eosin (H&E) and Safranin-O/Fast green (SOFG), Scale bars, 50  $\mu$ m. (d–f) Expression of Hsp6 (d), Atf4 (e), Grp78 (f) in articular cartilage were detected by immunohistochemistry, Scale bars, 50  $\mu$ m. (i) OARSI scoring was based on the results of SOFG staining. (j–l) Statistical graph of expression of Hsp6(j), Atf4(k), Grp78(l) detected by immunohistochemistry. (m) Schematic of the scientific hypothesis. MiR-3085-3p is upregulated in mechanical-loading chondrocytes and FJOA cartilage tissues directly related to endoplasmic reticulum stress and cell apoptosis. MiR-3085-3p induces ER stress by directly targeting Hsp6. \*\* $P < 0.01$ , \*\*\*\* $P < 0.0001$ . All data are shown as means  $\pm$  SD of six independent experiments in (g) (h) (i) (j) (k) (l), one-way analysis of variance (ANOVA) was used for comparison between multiple groups. (For interpretation of the references to colour in this figure legend, the reader is referred to the Web version of this article.)

elucidated, providing a promising direction for future research. Lastly, the detailed mechanism that mechanical stress induces the increase of miR-3085-3p remains further investigation.

In conclusion, the biological role of miR-3085-3p in FJOA development has been revealed by our study. An increased amount of miR3085-3p stimulates ER stress and leads to chondrocyte apoptosis. Intra-articular inhibition of miR-3085-3p may represent a novel and promising therapeutic strategy for FJOA.

#### Availability of detailed data and materials

The datasets used and analyzed during the current study are available from the corresponding author upon request.

#### Ethical approval

All experiments and interventions on animals comply with the ARRIVE guidelines, the U.K. Animals (Scientific Procedures) Act, 1986 and EU Directive 2010/63/EU for animal experiments. The Ethics Committee of the Nanfang Hospital of Southern Medical University approved the animal experiment (IACUC-LAC-20230411-009).

#### Credit author statement

Conception and design of the research: ZL, LW and ZZ; Data collection: JZ, YC, ZC and RT; Analysis and interpretation: ZL, CL, CF, and XX; Statistical analysis: ZL, CL and CF; Drafting manuscript: ZL and CL; Revision manuscript: XA, LW and ZZ. All authors contributed to manuscript revision, read, and approved the submitted version.

#### Funding

This work was supported by National Key R&D Program of China (No. 2022YFC2502900) and National Natural Science Foundation of China (82272527).

#### Declaration of competing interest

The authors declare that they have no competing interests.

#### Acknowledgements

We want to thank Central Laboratory of Nanfang Hospital (Southern Medical University, Guangzhou, Guangdong, China) for providing guidance and technical assistance in the study.

#### Appendix A. Supplementary data

Supplementary data to this article can be found online at <https://doi.org/10.1016/j.jot.2024.11.007>.

#### References

- Balague F, Mannion AF, Pellise F, Cedraschi C. Non-specific low back pain. *Lancet* 2012;379(9814):482–91.
- Chen S, Chen M, Wu X, Lin S, Tao C, Cao H, et al. Global, regional and national burden of low back pain 1990–2019: a systematic analysis of the Global Burden of Disease study 2019. *J Orthop Translat* 2022;32:49–58.
- Knezevic NN, Candido KD, Vlaeyen J, Van Zundert J, Cohen SP. Low back pain. *Lancet* 2021;398(10294):78–92.
- Romain P, Adrian K, Benjamin N, Jean-Michel P, Florence T, Arnaud A, et al. Facet joint syndrome: from diagnosis to interventional management. *Insights Imaging* 2018;9(5):773–89.
- Carvajal AG, Voirin-Hertz M, Garrigues F, Herbet M, Deloire L, Simon A, et al. Association of lumbosacral transitional vertebra and sacroiliitis in patients with inflammatory back pain suggesting axial spondyloarthritis. *Rheumatology* 2020;59(7):1679–83.
- Gellhorn AC, Katz JN, Suri P. Osteoarthritis of the spine: the facet joints. *Nat Rev Rheumatol* 2013;9(4):216–24.
- Chen D. Osteoarthritis: a complicated joint disease requiring extensive studies with multiple approaches. *J Orthop Translat* 2022;32:130.
- Du R, Xu G, Bai X, Li Z. Facet joint syndrome: pathophysiology, diagnosis, and treatment. *J Pain Res* 2022;15:3689–710.
- Anshul Malhotra N, Kumar A, Jyotsna Rohilla K, Sinha N. Comparative evaluation of intraarticular facet joint injection versus medial branch block in patients with low back pain: a randomised controlled study. *Cureus* 2023;15(11):e49232.
- Chen YS, Liu B, Gu F, Sima L. Radiofrequency denervation on lumbar facet joint pain in the elderly: a randomized controlled prospective trial. *Pain Physician* 2022;25(8):569–76.
- Moussa WM, Khedr W, Elsayw M. Percutaneous pulsed radiofrequency treatment of dorsal root ganglion for treatment of lumbar facet syndrome. *Clin Neurol Neurosurg* 2020;199:106253.
- Leclaire R, Fortin L, Lambert R, Bergeron YM, Rossignol M. Radiofrequency facet joint denervation in the treatment of low back pain: a placebo-controlled clinical trial to assess efficacy. *Spine* 2001;26(13): 1411–6, 1417.
- Cohen SP, Raja SN. Pathogenesis, diagnosis, and treatment of lumbar zygapophysial (facet) joint pain. *Anesthesiology* 2007;106(3):591–614.
- van Tilburg CW, Stronks DL, Groeneweg JG, Huygen FJ. Randomised sham-controlled double-blind multicentre clinical trial to ascertain the effect of percutaneous radiofrequency treatment for lumbar facet joint pain. *Bone Joint Lett J* 2016;98-B(11):1526–33.
- van Wijk RM, Geurts JW, Wynne HJ, Hammink E, Buskens E, Lousberg R, et al. Radiofrequency denervation of lumbar facet joints in the treatment of chronic low back pain: a randomized, double-blind, sham lesion-controlled trial. *Clin J Pain* 2005;21(4):335–44.
- Bao S. Mechanical stress. *Handb Clin Neurol* 2015;131:367–96.
- Liu Q, Hu X, Zhang X, Duan X, Yang P, Zhao F, et al. Effects of mechanical stress on chondrocyte phenotype and chondrocyte extracellular matrix expression. *Sci Rep* 2016;6:37268.
- Jaumard NV, Welch WC, Winkelstein BA. Spinal facet joint biomechanics and mechanotransduction in normal, injury and degenerative conditions. *J Biomech Eng* 2011;133(7):71010.
- Ao X, Wang L, Shao Y, Chen X, Zhang J, Chu J, et al. Development and characterization of a novel bipedal standing mouse model of intervertebral disc and facet joint degeneration. *Clin Orthop Relat Res* 2019;477(6):1492–504.
- Ameres SL, Zamore PD. Diversifying microRNA sequence and function. *Nat Rev Mol Cell Biol* 2013;14(8):475–88.
- Miyaki S, Asahara H. Macro view of microRNA function in osteoarthritis. *Nat Rev Rheumatol* 2012;8(9):543–52.
- Zhang H, Zheng W, Li D, Zheng J. miR-146a-5p promotes chondrocyte apoptosis and inhibits autophagy of osteoarthritis by targeting NUMB. *Cartilage* 2021;13(2 suppl):1467S–77S.
- Nakamura A, Rampersaud YR, Nakamura S, Sharma A, Zeng F, Rossomacha E, et al. microRNA-181a-5p antisense oligonucleotides attenuate osteoarthritis in facet and knee joints. *Ann Rheum Dis* 2019;78(1):111–21.
- Zhao J, Li C, Qin T, Jin Y, He R, Sun Y, et al. Mechanical overloading-induced miR-325-3p reduction promoted chondrocyte senescence and exacerbated facet joint degeneration. *Arthritis Res Ther* 2023;25(1):54.
- Crowe N, Swingle TE, Le LT, Barter MJ, Wheeler G, Pais H, et al. Detecting new microRNAs in human osteoarthritic chondrocytes identifies miR-3085 as a human, chondrocyte-selective, microRNA. *Osteoarthritis Cartilage* 2016;24(3):534–43.
- Le L, Niu L, Barter MJ, Young DA, Dalmay T, Clark IM, et al. The role of microRNA-3085 in chondrocyte function. *Sci Rep* 2020;10(1):21923.
- Briggs MD, Dennis EP, Dietmar HF, Pirog KA. New developments in chondrocyte ER stress and related diseases. *F1000Res* 2020;9.
- Rellmann Y, Eidfors E, Dreier R. Review: ER stress-induced cell death in osteoarthritic cartilage. *Cell Signal* 2021;78:109880.
- Kim C, Kim B. Anti-Cancer natural products and their bioactive compounds inducing ER stress-mediated apoptosis: a review. *Nutrients* 2018;10(8).
- Chen J, Chen J, Cheng Y, Fu Y, Zhao H, Tang M, et al. Mesenchymal stem cell-derived exosomes protect beta cells against hypoxia-induced apoptosis via miR-21 by alleviating ER stress and inhibiting p38 MAPK phosphorylation. *Stem Cell Res Ther* 2020;11(1):97.
- Grieco FA, Schiavo AA, Brozzi F, Juan-Mateu J, Bugliani M, Marchetti P, et al. The miRNAs miR-211-5p and miR-204-5p modulate ER stress in human beta cells. *J Mol Endocrinol* 2019;63(2):139–49.
- Liu X, Qian F, Fan Q, Lin L, He M, Li P, et al. NF-kappaB activation impedes the transdifferentiation of hypertrophic chondrocytes at the growth plate of mouse embryos in diabetic pregnancy. *J Orthop Translat* 2021;31:52–61.
- Luo J, Li H, Xiu J, Zeng J, Feng Z, Zhao H, et al. Elevated ZNF704 expression is associated with poor prognosis of uveal melanoma and promotes cancer cell growth by regulating AKT/mTOR signaling. *Biomark Res* 2023;11(1):38.
- D'Adamo S, Cetrullo S, Minguzzi M, Silvestri Y, Borzi RM, Flamigni F. MicroRNAs and autophagy: fine players in the control of chondrocyte homeostatic activities in osteoarthritis. *Oxid Med Cell Longev* 2017;2017:3720128.
- Jiang W, Chen H, Lin Y, Cheng K, Zhou D, Chen R, et al. Mechanical stress abnormalities promote chondrocyte senescence - the pathogenesis of knee osteoarthritis. *Biomed Pharmacother* 2023;167:115552.
- Dunn W, Duraine G, Reddi AH. Profiling microRNA expression in bovine articular cartilage and implications for mechanotransduction. *Arthritis Rheum* 2009;60(8): 2333–9.
- Yang X, Guan Y, Tian S, Wang Y, Sun K, Chen Q. Mechanical and IL-1beta responsive miR-365 contributes to osteoarthritis development by targeting histone deacetylase 4. *Int J Mol Sci* 2016;17(4):436.

- [38] Jin L, Zhao J, Jing W, Yan S, Wang X, Xiao C, et al. Role of miR-146a in human chondrocyte apoptosis in response to mechanical pressure injury in vitro. *Int J Mol Med* 2014;34(2):451–63.
- [39] Jakob U, Gaestel M, Engel K, Buchner J. Small heat shock proteins are molecular chaperones. *J Biol Chem* 1993;268(3):1517–20.
- [40] Bartelt-Kirbach B, Golenhofen N. Reaction of small heat-shock proteins to different kinds of cellular stress in cultured rat hippocampal neurons. *Cell Stress Chaperones* 2014;19(1):145–53.
- [41] Zeng L, Tan J, Lu T, Lei Q, Chen C, Hu Z. Small heat shock proteins and the endoplasmic reticulum: potential attractive therapeutic targets? *Curr Mol Med* 2015;15(1):38–46.
- [42] Lu T, Zou Y, Zhou X, Peng W, Hu Z. The mechanism on phosphorylation of Hsp20Ser16 inhibit GA stress and ER stress during OGD/R. *PLoS One* 2019;14(3): e213410.
- [43] Nahomi RB, Dimauro MA, Wang B, Nagaraj RH. Identification of peptides in human Hsp20 and Hsp27 that possess molecular chaperone and anti-apoptotic activities. *Biochem J* 2015;465(1):115–25.
- [44] Song Q, Liu X, Chen DJ, Lai Q, Tang B, Zhang B, et al. Evaluation of MRI and CT parameters to analyze the correlation between disc and facet joint degeneration in the lumbar three-joint complex. *Medicine (Baltim)* 2019;98(40):e17336.
- [45] Kettler A, Liakos L, Haegele B, Wilke HJ. Are the spines of calf, pig and sheep suitable models for pre-clinical implant tests? *Eur Spine J* 2007;16(12):2186–92.
- [46] Wang T, Pelletier MH, Christou C, Oliver R, Mobbs RJ, Walsh WR. A novel in vivo large animal model of lumbar spinal joint degeneration. *Spine J* 2018;18(10): 1896–909.